Distinct histone H3–H4 binding modes of sNASP reveal the basis for cooperation and competition of histone chaperones

Chao-Pei Liu,[1,4] Wenxing Jin,[1,4] Jie Hu,[1,2] Mingzhu Wang,[3] Jingjing Chen,[1] Guohong Li,[1,2] and Rui-Ming Xu[1,2]

[1]National Laboratory of Biomacromolecules, CAS Center for Excellence in Biomacromolecules, Institute of Biophysics, Chinese Academy of Sciences, Beijing 100101, China; [2]School of Life Science, University of Chinese Academy of Sciences, Beijing 100049, China; [3]Institutes of Physical Science and Information Technology, Anhui University, Hefei 230601, Anhui, China

Chromosomal duplication requires de novo assembly of nucleosomes from newly synthesized histones, and the process involves a dynamic network of interactions between histones and histone chaperones. sNASP and ASF1 are two major histone H3–H4 chaperones found in distinct and common complexes, yet how sNASP binds H3–H4 in the presence and absence of ASF1 remains unclear. Here we show that, in the presence of ASF1, sNASP principally recognizes a partially unfolded Nα region of histone H3, and in the absence of ASF1, an additional sNASP binding site becomes available in the core domain of the H3–H4 complex. Our study also implicates a critical role of the C-terminal tail of H4 in the transfer of H3–H4 between sNASP and ASF1 and the coiled-coil domain of sNASP in nucleosome assembly. These findings provide mechanistic insights into coordinated histone binding and transfer by histone chaperones.

[*Keywords*: histone; histone chaperone; NASP; ASF1; structure]

Supplemental material is available for this article.

Received October 10, 2021; revised version accepted November 2, 2021.

Genomic DNA in eukaryotes is packaged into chromatin with nucleosomes as the building block. Nucleosome core particles (NCP) are made up of an octamer of core histones, including two copies each of H3, H4, H2A, and H2B, wrapped around by ~146 bp of DNA (Luger et al. 1997). Each round of cell division demands the doubling of both DNA and histone content, with half of the histones being of parental origin and the other half newly synthesized, which are post-translationally modified prior to their deposition onto DNA (Ruiz-Carrillo et al. 1975; Sobel et al. 1995; Masumoto et al. 2005; Xu et al. 2005; Loyola et al. 2006; Han et al. 2007; Alvarez et al. 2011). A diverse set of histone chaperones form a chaperoning pathway coordinating virtually all histone activities from the cytoplasm to the nucleus (Das et al. 2010; Gurard-Levin et al. 2014; Grover et al. 2018; Pardal et al. 2019). In mammals, nuclear autoantigenic sperm protein (NASP), which is essential for chromosomal replication and cell cycle progression, plays important roles in histone homeostasis and nuclear translocation of H3–H4 together with the HAT1–RbAp46 histone acetyltransferase complex and another histone chaperone, antisilencing factor 1 (ASF1) (Verreault et al. 1998; Ai and Parthun 2004; Richardson et al. 2006; Campos et al. 2010; Jasencakova et al. 2010; Cook et al. 2011; Gurard-Levin et al. 2014).

NASP is evolutionarily conserved in eukaryotes (Dunleavy et al. 2007; Nabeel-Shah et al. 2014). Two isoforms are typically found in mammals, a longer testicular NASP (tNASP) is expressed in the testis, embryonic tissues, and certain transformed cells, and a shorter somatic NASP (sNASP) is ubiquitously present in mitotic cells (Richardson et al. 2000). In *X. laevis*, the NASP homolog N1/N2 is expressed in oocytes and specifically binds histone H3–H4 and maintains a pool of soluble histones required for DNA replication in the early embryo (Kleinschmidt and Franke 1982; Kleinschmidt et al. 1985; O'Rand et al. 1992). *S. pombe* Sim3 (start independent of mitosis 3) and *S. cerevisiae* Hif1 (histone acetyltransferase 1 interacting factor 1) are two yeast homologs of human NASP (Ai and Parthun 2004; Dunleavy et al. 2007). Together, they form the SHNi-TPR (Sim3–Hif1–NASP interrupted tetratricopeptide repeat) protein family

[4]**These authors contributed equally to this work.**
Corresponding authors: rmxu@ibp.ac.cn, liuchaopei@ibp.ac.cn
Article published online ahead of print. Article and publication date are online at http://www.genesdev.org/cgi/doi/10.1101/gad.349100.121.

characterized by the presence of tandem tetratricopeptide repeat (TPR) motifs interrupted with an insertion (Dunleavy et al. 2007). NASP proteins have four TPR motifs, and the structure of yeast Hif1 displays that the four tandem TPR motifs form an arch, and two Hif1 molecules bind to one H2A–H2B dimer (Liu et al. 2014; Zhang et al. 2016).

Human sNASP is a 449-residue protein essential for cellular DNA replication, cell cycle progression, and embryonic development (Richardson et al. 2006; Alekseev et al. 2009, 2011; Cook et al. 2011). During normal cell cycle progression, the expressed level of NASP is under tight control, as overexpression of NASP leads to a delay in the progression though the G1/S border (Cook et al. 2011). sNASP was initially implicated as a chaperone of linker histone H1 involved in the assembly and disassembly of higher-order chromatin structure (Richardson et al. 2000; Finn et al. 2008, 2012). Through mass spectrometry analysis and biochemical fractionations, it was later found to be in both cytosolic and nuclear complexes together with ASF1 (Campos et al. 2010; Jasencakova et al. 2010; Apta-Smith et al. 2018). Previous studies revealed that sNASP serves to maintain a soluble reservoir of mature H3–H4 histone proteins (Cook et al. 2011), facilitates rapid and efficient transport of histones into the nucleus, and promotes nucleosome assembly with histone H3–H4 (Tyler et al. 1999; Wang et al. 2008, 2012; Osakabe et al. 2010). At present, limited information about how sNASP interacts with H3–H4 and how sNASP passes histone H3–H4 to ASF1 is known. It is reported that sNASP can form a quaternary complex with ASF1A and H3–H4. A recent study revealed that the TPR4 motif of sNASP binds a seven-amino-acid peptide motif at the globular H3 C-terminal region with high affinity (Bowman et al. 2016), and that the C-terminal region of histone H3 interacts with ASF1 (Bowman et al. 2017). Nonetheless, an overall picture of how sNASP binds H3–H4 and cooperates with ASF1 for transfer of H3–H4 remains enigmatic.

Here we present a combined structural and biochemical analysis, revealing that sNASP specifically recognizes histone H3–H4 principally through the N-terminal tail of histone H3 in the presence of ASF1, whereas a different binding mode emerges in the absence of ASF1. These findings provide mechanistic insights into key steps of cytoplasmic histone processing and transfer pathways.

Results

sNASP exists in monomeric and dimeric forms

The conserved core of human sNASP consists of a TPR domain with four tandem TPR motifs, among which the second TPR is interrupted by a large acidic (DE-rich) region, and a coiled-coil (CC) domain follows the C-terminal end of TPR4 (Fig. 1A). We expressed the sNASP TPR domain (amino acids 40–320) in bacteria as a poly(histidine)-sumo-tagged fusion protein, and purified the protein through successive Ni^{2+}-chelating, sumo tag cleavage and size exclusion column chromatography steps. We noticed that sNASP eluted from the sizing column in two separated peaks (Fig. 1B). The two populations of sNASP are relatively stable, as pooling three peak fractions from each peak and running them through the sizing column again separately shows that the peak 1 sample remain eluted at the same volume, whereas a small but noticeable amount of the peak 2 sample dispersed over to the peak 1 position (Fig. 1B). The two-peak elution profile is preserved at 100 mM salt concentration, although with different relative abundances (Supplemental Fig. S1A). Analytical ultracentrifugation (AUC) studies revealed that peak 1 is predominantly made up of sNASP dimers, whereas peak 2 is a mixture of sNASP monomers and a small fraction of dimers, judged by their theoretical molecular masses of 30 kDa and 60 kDa, respectively (Fig. 1C).

To know whether full-length sNASP also exists in two oligomeric forms, we expressed full-length sNASP with a C-terminal strep tag in HEK293F cells. Following affinity and ion exchange purification steps, size exclusion chromatography analysis revealed that full-length sNASP also eluted in two peaks, although the later peak is considerably more abundant (Fig. 1D). An AUC analysis shows that the major peak contains mostly sNASP monomers, which has a molecular mass of ~53 kDa, and a very small amount of sNASP dimers, which has a molecular mass of 105 kDa (Fig. 1E). Altogether, we found that purified sNASP exists in both monomeric and homodimeric forms.

Homodimeric structure of sNASP

We first wished to determine the structures of sNASP in monomeric and dimeric forms in order to gain insights into how they bind histones. Crystallization of both forms of sNASP TPR domain was attempted; however, only the dimeric protein crystallized, and a 2.9 Å structure was solved (Fig. 2A; Table 1). There is one sNASP molecule per asymmetric unit, and an apparent homodimer results from the packing of a twofold crystallographic symmetry-related molecule via an ~60-residue C-terminal helix. Surprisingly, this long helix is formed by the predicted second helix of the TPR4 motif and the entire coiled-coil domain. Apart from this long C-terminal helix, each of the TPR units from 1 to 3 consists of two antiparallel α helices, while TPR4 has a separate N-terminal helix (Fig. 2A). For ease of description, we denote these helices α1 to α7 sequentially from the N terminus, and the long C-terminal helix is termed αC, which is further separated into an N-terminal α8 segment belonging to the TPR4 motif, and a C-terminal α9 segment, which corresponds to the predicted coiled-coil domain (Fig. 2A). Homodimerization of sNASP entails the formation of an extended antiparallel coiled-coil between the two αC helices, and the intermolecular interaction buries a surface area of 1877 $Å^2$. The coiled-coil interaction involves six pairs of charged residues and a number of hydrophobic ones (Supplemental Fig. S1B). Not surprisingly, removal of αC impairs the dimerization ability of sNASP in solution (Supplemental Fig. S1C).

The TPR motifs pack via stacking of the N-terminal helix of the next TPR motif onto the groove between the helix pair of the preceding TPR motif, principally via

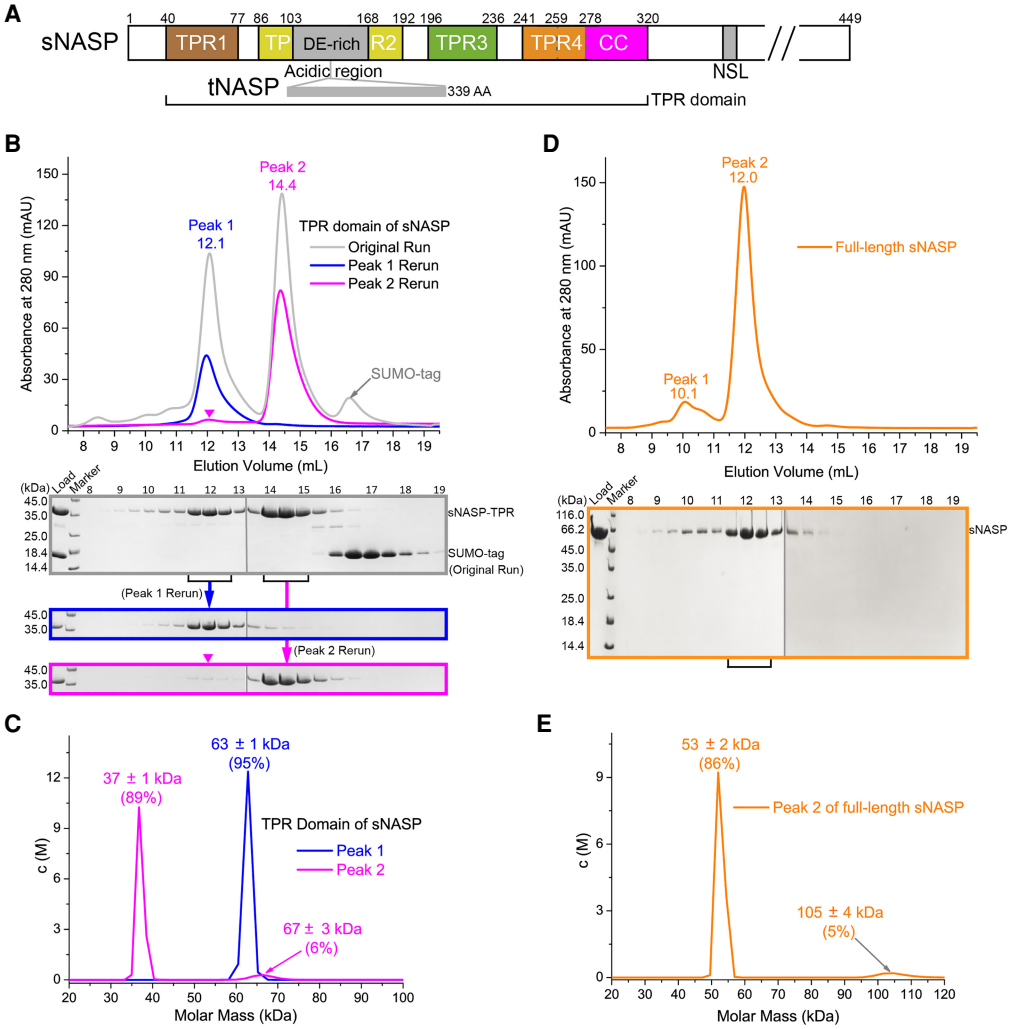

Figure 1. Oligomeric state of sNASP. (*A*) A schematic diagram depicting TPR1-4 motifs and acidic (DE-rich), coiled-coil (CC), and nuclear localization signal (NLS) regions of sNASP. A 339-residue insertion in the acidic region constituting tNASP is also indicated. (*B*) Two-hundred-eighty-nanometer absorbance elution profiles of sNASP TPR from a Superdex 200 increase 10/300 GL size exclusion column. The gray line indicates the profile from the sample after nickel-chelating purification and sumo tag cleavage. Blue and magenta lines represent profiles from a second run using the fractions pooled from peak 1 (11.5–13.0 mL) and peak 2 (14.0–15.5 mL), respectively. Each 0.5-mL elution fraction, spanning 8.0–19.5 mL, for all three runs was analyzed by SDS-PAGE and is shown *below*. Gel panels, each of which was assembled from two gels with their boundary indicated by a thin vertical gray line, from the first run, rerun of peak 1, and peak 2 are arranged from *top* to *bottom*, and aligned according to elute fractions (numbered *above* the *top* panel). A magenta inverted triangle indicates the presence of a small peak at the peak 1 position in the rerun of peak 2 sample. (*C*) AUC analysis of peak 1 (blue) and peak 2 (pink) samples. Sedimentation velocity measurement of molecular mass distribution, c(M) in 10^{-2}/kDa, is plotted. (*D*) Gel filtration analysis of full-length sNASP expressed in HEK293F cells. The gel panel was assembled from two gels separated by a thin vertical gray line. (*E*) AUC analysis of the peak 2 fractions (11.0–13.0 mL) of full-length sNASP.

hydrophobic interactions, and the packing results in a right-handed superhelical twist (Fig. 2A). While charge distribution on the inner (concave) surface of the TPR domain is mainly neutral, the exposed surface of α1, which forms one rim of the concave surface, is positively charged (Fig. 2B). In contrast, the loop connecting α3 and α4 in TPR2 and that connecting α5 and α6 in TPR3, both of which are part of the convex side of the sNASP surface, are negatively charged. Additionally, a 63-residue segment of the DE-rich region, which is inserted between α3 and α4, is disordered in the structure. It is interesting that the approximately seven C-terminal turns of the long αC are highly charged, but oppositely charged residues are segregated on the opposing surface sides along the C-terminal segment of αC, and the negatively charged surface region from the symmetry-related sNASP molecule forms the other rim of the concave surface sNASP (Fig. 2B). Previous studies showed that the TPR domain of sNASP is capable of binding histone H3–H4 and possesses the nucleosome assembly activity in vitro (Osakabe et al. 2010; Bowman et al. 2016, 2017), while the coiled-coil domain may provide a structural scaffold mediating protein–protein

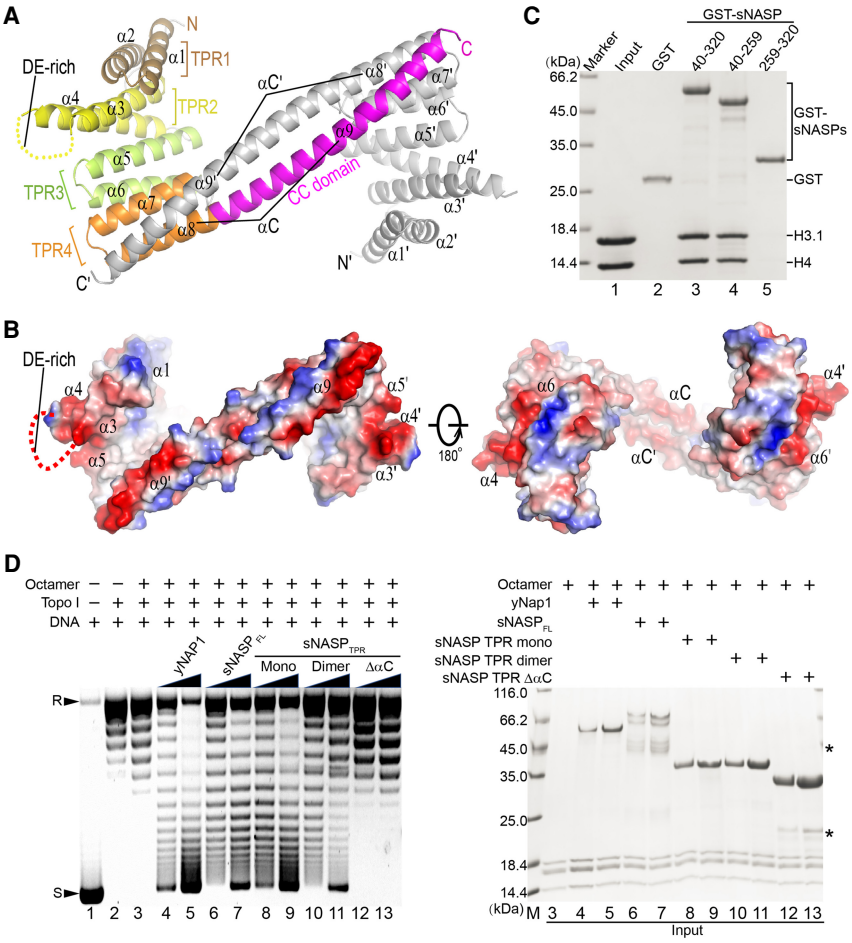

Figure 2. Homodimeric structure of sNASP. (*A*) A cartoon representation of the sNASP TPR domain dimer. One molecule is colored according to the TPR repeat motifs (α1–α8) as indicated, and the CC domain (α9) is in magenta. The symmetry-related molecule is colored gray. The two sNASP TPR molecules dimerize via antiparallel packing of the long αC helix, which is composed of α8 and α9. (*B*) Electrostatic potential of homodimer surface viewed from two directions related by 180° rotation. Uncharged and negatively and positively charged surface regions are colored white, red, and blue, respectively. (*C*) Pull-downs of histone H3.1–H4 with GST-tagged sNASP fragments (TPR, amino acids 40–320; TPRΔαC, amino acids 40–259; and αC, amino acids 259–320) analyzed by Coomassie-stained SDS-PAGE. (*D*) Supercoiling assay for in vitro nucleosome assembly by sNASP. (*Left*) ϕX174 DNA (lane *1*) was treated with DNA topoisomerase I (lane *2*) and incubated with histone octamers (lane *3*, negative control), and increasing amounts (0.25 and 0.5 µg) of yNap1 (lanes *4,5*, positive control), full-length sNASP (lanes *6,7*), sNASP TPR monomer (lanes *8,9*), dimer (lanes *10,11*), and the ΔαC variant (lanes *12,13*), together with 0.2 µg of histone octamer, were incubated with 0.1 µg of relaxed ϕX174 DNA. Arrowheads labeled R and S at the *left* indicate positions of supercoiled and relaxed DNA. (*Right*) Input protein samples for the supercoiling assay analyzed by Coomassie-stained SDS-PAGE.

interactions (Rose and Meier 2004). Our GST pull-down assay indicates that both the intact sNASP TPR domain (Fig. 2C, lane 3), which is mixture of monomeric and dimeric forms, and its homodimerization-defective truncation variant encompassing α1–α7 (Fig. 2C, lane 4) can interact with histone H3.1–H4, whereas the C-terminal long helix αC (amino acids 259–320), which contains TPR4 α8 and the CC domain, cannot (Fig. 2C, lane 5). Interestingly, we found that, although not needed for H3–H4 binding, the coiled-coil domain of sNASP is important for its nucleosome assembly activity, as judged by an in vitro supercoiling assay (Fig. 2D). In this assay, both monomeric and dimeric forms of the sNASP TPR domain appear to have levels of nucleosome assembly activity comparable with that of the full-length protein.

Structure of monomeric sNASP in complex with H3–H4 and ASF1

sNASP has been shown to form a quaternary complex with histones H3 and H4 and their chaperone ASF1 (Bowman et al. 2017). To investigate how sNASP binds histone H3–H4 together with ASF1, we assembled the quaternary complex using the sNASP TPR domain, the globular domain of ASF1A (amino acids 1–172), and full-length histones H3.1 and H4 under a medium salt concentration condition (0.5 M NaCl). Gel filtration results showed that both dimeric and monomeric forms of the sNASP TPR domain can form stable complexes with the preassembled ASF1A–H3.1–H4 complex. They eluted from a Superdex 200 10/300GL sizing column at ~11- and 13-mL elution volume, respectively, while the ASF1A–H3.1–H4 complex eluted at ~14.7 mL (Fig. 3A). However, crystallization trials of the two sNASP-containing complexes with a large number of conditions were unfruitful.

We reasoned that one possible reason for unsuccessful crystallization might be due to ASF1A–H3–H4's propensity to precipitate under low salt concentrations (<0.5 M NaCl). To overcome this problem, we engineered a fusion protein in which the globular domain of ASF1A (amino acids 1–156) is tethered to the C-terminal end of the sNASP TPR domain through a 20-residue GS linker, with the sequence of four repeats of GGGGS. The sNASP–ASF1A fusion protein was then coexpressed with full-length human H3.1 and H4 in *E. coli*, and the complexes with H3.1–H4 were also stable at 0.5 M NaCl. Furthermore, the fusion protein forms monomeric and dimeric complexes with H3.1–H4 much like the corresponding complexes assembled with separately expressed sNASP and ASF1A (Supplemental Fig. S2A), and now the fusion protein complexes can tolerate a low salt concentration, even at 100 mM NaCl. Importantly, we were able to achieve

Table 1. *Data collection and refinement statistics*

	sNASP^{TPR} SeMet	sNASP^{TPR} native	sNASP^{TPR}–$(G_4S)_4$–ASF1A$_{1–156}$–H3.1–H4 complex
Data collection			
Wavelength (Å)	0.97915	0.97915	0.97913
Space group	$P6_222$	$P6_222$	P1
Cell dimensions			
a, b, c (Å)	96.14, 96.14, 208.87	96.83, 96.83, 209.33	71.13, 71.00, 104.39
α, β, γ (°)	90, 90, 120	90, 90, 120	105.32, 101.99, 95.75
Resolution (Å)	50.00–3.60 (3.73–3.60)[a]	50.00–2.90 (3.00–2.90)[a]	50.00–3.00 (3.11–3.00)[a]
R_{merge}	0.134 (0.687)	0.061 (0.876)	0.096 (0.569)
I/σI	19.4 (5.4)	31.1 (2.6)	13.9 (2.3)
Completeness (%)	99.7 (100)	98.5 (99.1)	90.7 (92.3)
Redundancy	17.4 (18.1)	8.0 (8.3)	3.8 (3.9)
Total/unique reflections	124,473/7154	105,828/13,286	134,115/33,846
Refinement			
Resolution (Å)		15.00–2.90	15.00–3.00
Number of reflections		13,042 (2280)	33,326 (1865)
R_{work}/R_{free}		0.187/0.223	0.165/0.203
Number of atoms		1848	8594
Protein residues		220	1071
Ligand/Ion		9	8
Water		30	44
B factors (Å^2)			
Protein		63.5	73.5
Ligand/ion		94.1	83.8
Water		54.2	44.1
RMS deviations			
Bond lengths (Å)		0.009	0.003
Bond angles (°)		0.925	0.54
Ramachandran plot			
Favored		97.2%	97.4%
Allowed		2.8%	2.6%
Outliers		0	0

[a]Values in parentheses are for highest-resolution shell.

crystallization of the sNASP–ASF1A–H3–H4 complex using the monomeric fusion protein, and succeeded in solving a 3.0-Å resolution structure by molecular replacement (Fig. 3B; Table 1). There are two sNASP–ASF1A–H3–H4 complexes, both with a 1:1:1:1 subunit stoichiometry, in the crystallographic asymmetric unit (ASU). The two complexes within the ASU share a highly similar structure, manifested by an overall root-mean-square deviation (RMSD) of 0.16 Å. The contacts between the two complexes within the ASU are mediated through ASF1–ASF1 interactions and do not appear to have physiological implications. Thus, we will choose the complex (chains A–D) having a better quality electron density map for further analysis from now on.

In the structure, the electron density for the GS linker is completely absent, and the C-terminal end of sNASP and the N-terminal end of ASF1A to which the GS linker connects are spatially close (Fig. 3B). This observation indicates that the linker has a flexible conformation, and artificial tethering of sNASP and ASF1A via this linker did not constrain their positioning for histone binding. The structure shows that sNASP makes direct contacts with both histones H3 and H4, which bind ASF1A as a heterodimer in the same manner as seen in the structures of ASF1–H3–H4 complexes (Fig. 3B,C; English et al. 2006; Natsume et al. 2007; Zhang et al. 2018). sNASP interacts with histones H3 and H4 through the convex surface of the TPR domain: TPR1 through TPR3 with H3, and TPR3–TPR4 with H4 (Fig. 3B). Intriguingly, histone H3 interacts with sNASP principally via its N-terminal flexible region encompassing residues 40–57, which normally adopts a helical structure (αN) in NCP. The conformation of this H3 region is highly variable outside the nucleosomal context, and αN is mostly unwound in the present structure (Fig. 3D). Previous structural studies found that αN could adopt different orientations when binding histone chaperones, but the helical structure remains mostly intact. The drastic structural change of αN in histone H3 was first observed in the structure of Rtt109, a yeast H3K56 acetyltransferase, bound to the Asf1–H3–H4 complex (Zhang et al. 2018). Our observation here reinforces the notion that conformational dynamics of this H3 region are important for recognition by histone chaperones. The very N-terminal 39 residues of H3 are disordered, but based on the location of the ordered portion of the H3 N-terminal tail from residue 40 onward, the disordered portion of the H3 N-terminal tail is expected to be in the vicinity of the also disordered DE-rich acidic region between α3 and α4 of sNASP (Fig. 3B). The oppositely charged H3 tail and

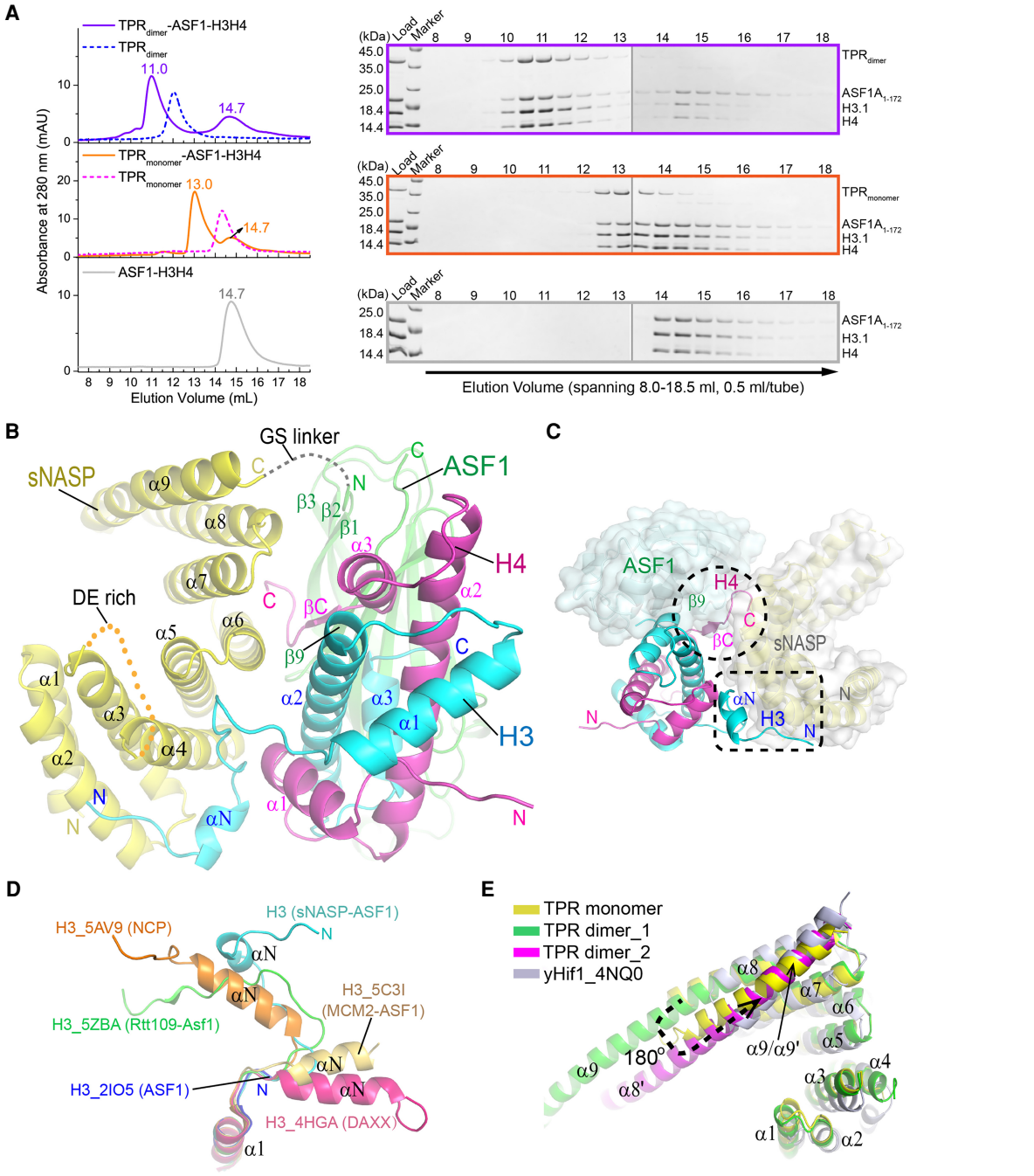

Figure 3. Structure of the monomeric sNASP bound to H3–H4 and ASF1A. (*A*, *left* panels) Sizing column elution profiles of dimeric (*top* panel) and monomeric (*middle* panel) sNASP TPR domain with the ASF1-H3–H4 complex, and the ASF1A–H3–H4 complex alone (*bottom*). The profiles of sNASP dimers and monomers, shown in blue and magenta dashed lines, are superimposed for reference in respective panels. (*Right* panels) SDS-PAGE analysis of 0.5-mL fractions spanning the 8.0- to 18.5-mL elution volume corresponding to the three sizing column runs displayed in the *left* panels, respectively. Each gel panel was assembled from two gels with a thin vertical gray line separating them. (*B*) Overall structure of the sNASP–ASF1A–H3–H4 quaternary complex. sNASP is colored yellow, ASF1A is colored green, H3 is colored cyan, and H4 is colored magenta. Orange dashed line denotes the disordered DE-rich region within TPR2, and the gray dashed line indicates the disordered GS linker joining sNASP and ASF1A. (*C*) A top view of the structure in cartoon drawing superimposed with a semitransparent surface representation of sNASP (gray) and ASF1A (light green). sNASP regions involved in binding the N-terminal segment of H3 and the C-terminal tail of H4 are indicated with a dashed rectangle and circle, respectively. (*D*) Conformational differences of the N-terminal region of H3 in the structures with the sNASP–ASF1 complex (cyan), nucleosome core particle (NCP, orange) (PDB: 5AV9), the Rtt109-Asf1 complex (green) (PDB: 5ZBA), the MCM2-ASF1 complex (yellow) (PDB: 5C3I), ASF1 (light blue) (PDB: 2IO5), and DAXX (magenta) (PDB: 4HGA). (*E*) Superposition of the sNASP TPR monomer structure, colored the same as above, with that of the sNASP dimer, colored green and magenta, and yeast Hif1 (PDB: 4NQ0) colored in gray.

the acidic region of sNASP may interact via Coulomb's force. Additionally, histone H4 interacts with sNASP via its C-terminal β strand, which is stabilized by interaction with ASF1A, and the very C-terminal tail (Fig. 3B,C; Supplemental Fig. S2B).

The sNASP TPR domain in the complex structure is apparently in a monomeric form, and its structure is very similar to that of the yeast Hif1 monomer; the two can be superimposed with an RMSD of 2.18 Å. The structures of monomeric and dimeric forms of sNASP are nearly identical throughout the four TPR motifs, except that the very C-terminal helix α9, which joins with α8 to form the long, continuous αC in the dimeric structure of sNASP, folds back to form an antiparallel coiled coil with α8 in the present structure (Fig. 3E). Apart from this difference, the two TPR domain structures can be superimposed with an RMSD of 0.57 Å.

Interaction between sNASP and H3–H4

The structure shows that the N-terminal segment of histone H3 (amino acids 40–57) snakes through the convex surface of sNASP formed by TPR1, TPR2, and TPR3 (Fig. 4A), as evidenced by a clear, continuous electron density map (Supplemental Fig. S3A). This region of histone H3 interacts with sNASP extensively through a mixture of hydrophobic interactions, salt bridges, and hydrogen bonds (Fig. 4A). Outside the N-terminal region of H3, only Glu105 in the central α2 helix of H3 is found to interact with sNASP via hydrogen bonding to Gln221 and Glu224 located in α6 of TPR3. We deleted the entire N-terminal tail (amino acids 1–60) of histone H3.1 (H3.1Δ60) and tested the interaction between the sNASP TPR domain and H3.1Δ60–H4 in the presence and absence of ASF1A. GST pull-down results (Fig. 4B) show that the sNASP TPR domain dramatically reduced binding with ASF1A–H3.1Δ60–H4 (Fig. 4B, lane 13), whereas no obvious impact is observed with full-length H3.1–H4, alone (Fig. 4B, lane 10) or in complex with ASF1A (Fig. 4B, lane 12), and H3.1Δ60–H4 (Fig. 4B, lane 11). This observation validates the structural finding that the N-terminal tail of histone H3 is essential for sNASP binding when ASF1 is present, and also reveals that sNASP binds H3–H4 differently when ASF1 is absent.

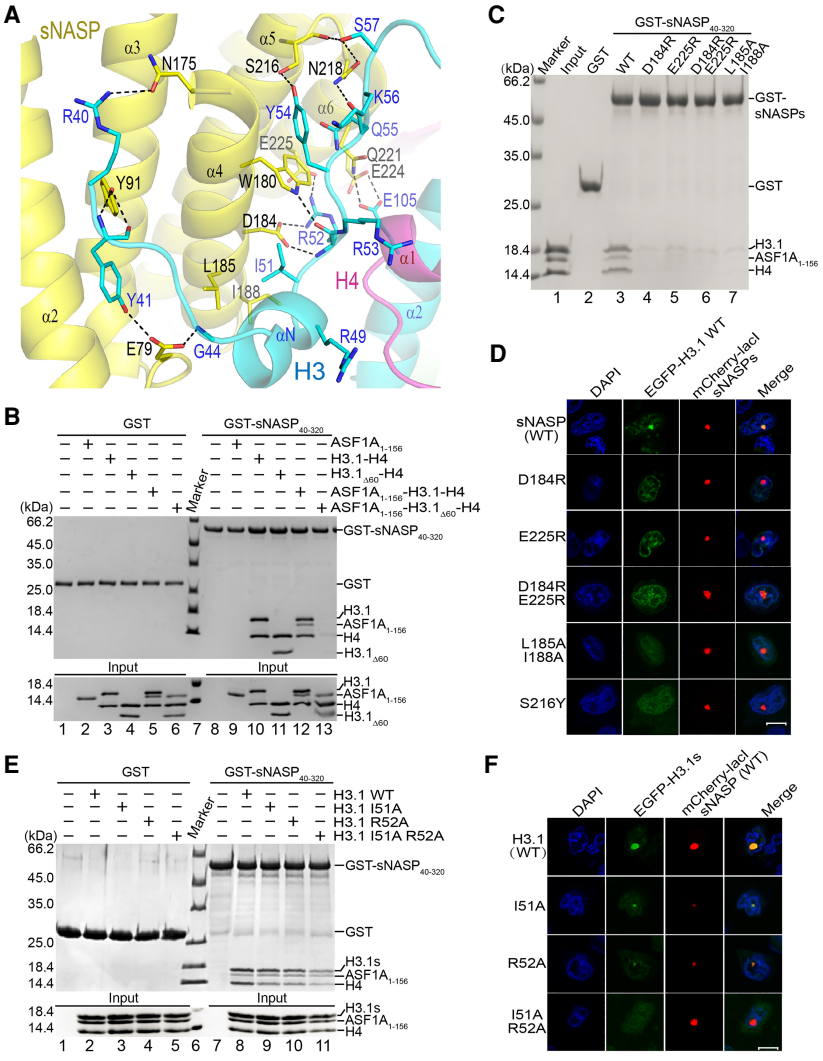

Figure 4. Histone H3 N-terminal tail binding sites in sNASP. (*A*) Detailed view of interactions between residues 40–57 of histone H3 (cyan) and sNASP TPR (yellow). The involved residues are shown in a stick representation, with sNASP and H3 residues labeled in black and blue, respectively, and black dashed lines indicate hydrogen bonds. (*B*, *top* panel) Pull-down of protein samples indicated with a plus sign by the GST-tagged sNASP TPR domain or GST. (*Bottom* panel) Input samples for GST pull-down experiments. Corresponding lane numbers are labeled at the *bottom*. (*C*) GST pull-down of the ASF1A–H3.1–H4 complex by sNASP or its indicated mutants. (*D*) Cellular colocalization test of WT or mutant sNASP with H3.1. Scale bar, 10 µm. (*E*) GST pull-down of H3.1 and its mutants by sNASP. (*F*) Colocalization test of sNASP with H3.1 and its indicated mutants.

To further delineate sNASP–H3 interactions, we carried out structure-guided mutagenesis of sNASP and tested the binding of these mutants to the ASF1A–H3.1–H4 complex. Prominently among sNASP–H3 interactions, Ile51 of H3 contacts Leu185 and Ile188 located in α4 of sNASP via hydrophobic interactions; and the guanidino group of Arg52 of H3 interacts with Asp184 in α4 and Glu225 in α6 of sNASP via hydrogen bonds and charge interactions, while the carbonyl of Arg52 makes a hydrogen bond with the nitrogen atom of the indole ring of Trp180 of sNASP. GST pull-downs with the D184R, E225R, D184R E225R, or L185A I188A mutants of sNASP show that these mutants effectively lost binding to the ASF1A–H3–H4 complex (Fig. 4C, lanes 4–7). These in vitro pull-down results are supported by LacO-LacI targeting experiments in mammalian A03_1 cells, where sNASP or its derivatives were fused with mCherry and LacI, while H3.1 was fused to EGFP (Fig. 4D; Supplemental Fig. S3B, C). Reciprocally, we made I51A, R52A, and I51A R52A mutants of H3, and GST pull-down experiments showed that the individual I51A or R52A mutations have minimal impact on sNASP–H3 binding, while the I51A R52A combination mutant of H3 greatly impaired the interaction with sNASP (Fig. 4E, lanes 9–11). The in vitro GST pull-down results are corroborated by cellular targeting experiments (Fig. 4F; Supplemental Fig. S3D). It is worth pointing out that Ile51 and Arg52 are strictly conserved among histone variants across species (Supplemental Fig. S3E), suggesting a common sNASP binding mode of H3 variants in the presence of ASF1.

In addition to the above-mentioned sNASP–H3 interactions, the hydroxyl and the carbonyl groups of Ser216 of sNASP make hydrogen bonds with Tyr54 and Ser57 of H3, respectively. Ser57 of H3 also contacts Asn218 of sNASP via a hydrogen bond. Tyr41 of H3 interacts with Glu79 and Tyr91 of sNASP, and Asn175 of sNASP forms a hydrogen bond with Arg40 of H3 (Fig. 4A). Interestingly, a S216Y change is among somatic mutations of sNASP in cancer tabulated in the COSMIC database (Bamford et al. 2004). A GST pull-down of the ASF1A–H3–H4 complex by the S216Y mutant of sNASP showed no obvious effect, while cellular targeting experiments showed noticeable reduction of colocalization of the sNASP mutant with histone H3 (Fig. 4D; Supplemental Figs. S3C, S4A). This result indicates a possible link between histone binding and human pathogenesis by sNASP alterations. As a contrast, certain sNASP or H3.1 mutations at the interface between the two showed minimal or no impact on sNASP–histone interaction (Supplemental Fig. S4), thus rendering support of the significance of our earlier analyses.

The sNASP interaction region of histone H4 is located in the C-terminal tail of histone H4 (amino acids 95–102), which is visible in its entirety in the structure. Residues 95–97 form an antiparallel β sheet with ASF1A, and the side chain of Phe100 inserts into a hydrophobic pocket between two β sheets of ASF1A (Fig. 5A; Supplemental Fig. S5A). In this area, we noted the only direct interaction between ASF1A and sNASP involved a hydrogen bond between Asn231 of sNASP and ASF1A Ser142's main chain carbonyl group. The sole function of ASF1A appears to be to stabilize the C-terminal residues of H4, thus enabling them to participate in intermolecular interactions. A similar mechanism of Asf1 was noted in the previous study of its function in regulating H3K56 acetylation of Rtt109 (Zhang et al. 2018).

sNASP–H4 interactions involve hydrogen bonds between Tyr255 of sNASP and Arg95 and the C-terminal carboxylate of Gly102 of H4, Glu263 of sNASP and Arg95 of H4, and Gln267 of sNASP and the carbonyl group of Gly101 of H4. To test their significances, we created a sNASP Y255R Q267R double mutant and an H4 deletion mutant, H4Δ95-C, removing all residues from Arg95 to the C terminus. However, both cellular targeting and in vitro GST pull-down assays show that these mutations of sNASP and H4 do not compromise the binding between sNASP and histones H3–H4 (Fig. 5B; Supplemental Fig. S5B,C). Curiously, we noticed that in the GST pull-down experiments with the ASF1A–H3–H4Δ95-C complex, ASF1A is evicted from the sNASP–histone complex (Fig. 5B, lane 6). Gel filtration experiments also show that both monomeric and dimeric forms of the sNASP TPR domain can evict ASF1A from the ASF1A–H3–H4Δ95-C complex (Fig. 5C). These results indicate that while the interaction between sNASP and the C-terminal tail of H4 is of marginal effect, it is important for ASF1A to maintain a firm grip on H3–H4 in the presence of sNASP, which appears to be able to compete ASF1A off H3–H4 through binding to a yet unidentified site in H3–H4 either overlapping with the ASF1A binding sites or through an allosteric effect.

Histone binding mode of sNASP in the absence of ASF1

Our earlier GST pull-down experiments showed that while deletion of the N-terminal 60 residues of histone H3 impaired the binding with sNASP in the context of the ASF1A–H3Δ60–H4 complex, the binding of H3Δ60–H4 to sNASP is unaffected (Fig. 4B). Since the GST pull-down result cannot distinguish whether the dimeric, monomeric, or both forms of sNASP was responsible for binding H3Δ60–H4 in the absence of ASF1A, we used sizing column to resolve this puzzle. Figure 6A shows that both dimeric and monomeric forms of sNASP bind H3Δ60–H4 in the absence of ASF1A. These observations implicate the presence of additional sNASP binding sites in the H3.1–H4 complex that were not accessible when ASF1A was bound. A reciprocal question is which part of sNASP is involved in H3–H4 binding in this case, and by structure-guided systematic deletions we tried to map the extra H3–H4 binding region of sNASP. To avoid complications in interpreting binding data, the N-terminal tail-deleted H3Δ60 complex with H4 is used in our GST pull-down analyses. Six sNASP fragments, as schematically shown in the left panel of Figure 6B, were fused to GST and used to pull down H3.1Δ60–H4. As shown in lanes 3, 7, and 9 in the right panel of Figure 6B, significant histone binding was detected with the three sNASP fragments, all containing TPR4 and the CC domain, while the TPR1 (lane 5) and TPR3 (lane 8) fragments showed no binding. It is worth pointing out that the CC domain and α8 of TPR4 were

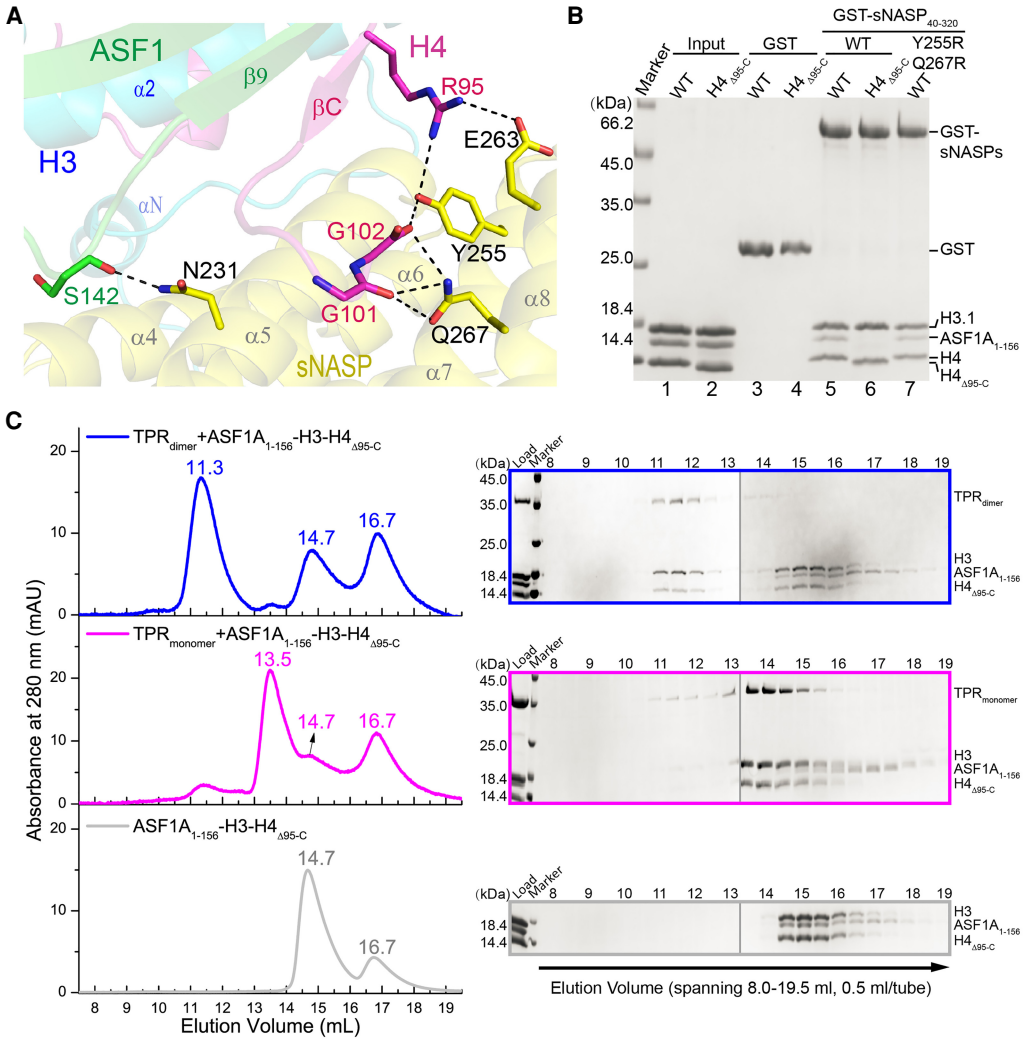

Figure 5. Interaction between sNASP and histone H4. (*A*) Depiction of interactions involving H4 C-terminal tail encompassing residues 95–102 (magenta), ASF1 (green), and sNASP (yellow). The involved residues are shown in a stick representation, and black dashed lines indicate hydrogen bonds. (*B*) GST pull-down of ASF1A–H3.1–H4 or ASF1A–H3.1–H4Δ95-C complexes by the WT or Y255R Q267R mutant of sNASP. (*C*, *left* panels) From *top* to *bottom*, sizing column elution profiles of the ASF1A–H3–H4Δ95-C complex with dimeric and monomeric sNASP and without sNASP, respectively. (*Right* panels) From *top* to *bottom*, SDS-PAGE analysis of 0.5-mL fractions spanning 8.0–19.5 mL corresponding to three column runs shown in the *left* panels. Each gel panel was assembled from two gels with their boundary indicated by a thin vertical gray line.

shown not to interact with H3.1–H4 earlier (Fig. 2C, lane 5), leaving α7 of TPR4 as the principal element for histone binding in the absence of ASF1. The TPR2 (Fig. 6B, lane 6) and TPR2-containing TPR1-2 (Fig. 6B, lane 4) fragments displayed significantly weakened but detectable bindings. In the structure of sNASP with ASF1A–H3–H4, TPR2 is involved in interaction with the N-terminal tail of H3, while TPR4 interacts with the C-terminal of H4, although the latter interaction was not essential for complex formation. It is also worth pointing out that TPR2 contains the DE-rich acidic region, and residual interaction with tailless H3 seen in lanes 4 and 6 of Figure 6B is also unexpected from the complex structure of sNASP–ASF1–H3–H4 (Fig. 3B). Altogether, the detection of TPR2 and α7 of TPR4 in binding the H3–tailless H3.1Δ60–H4 complex indicates the existence of a different histone binding mode of sNASP in the absence of ASF1A.

Discussion

The central functions of histones in the organization, dynamics, and biogenesis of eukaryotic genomes require special biochemical and biophysical properties of these proteins. Some prominent features of these proteins include having large number of charged residues, flexible terminal tails, and modular core domains capable of ordered assembly into defined oligomers. However, these functionally important properties also introduce potential harmful effects, such as tendency to aggregate,

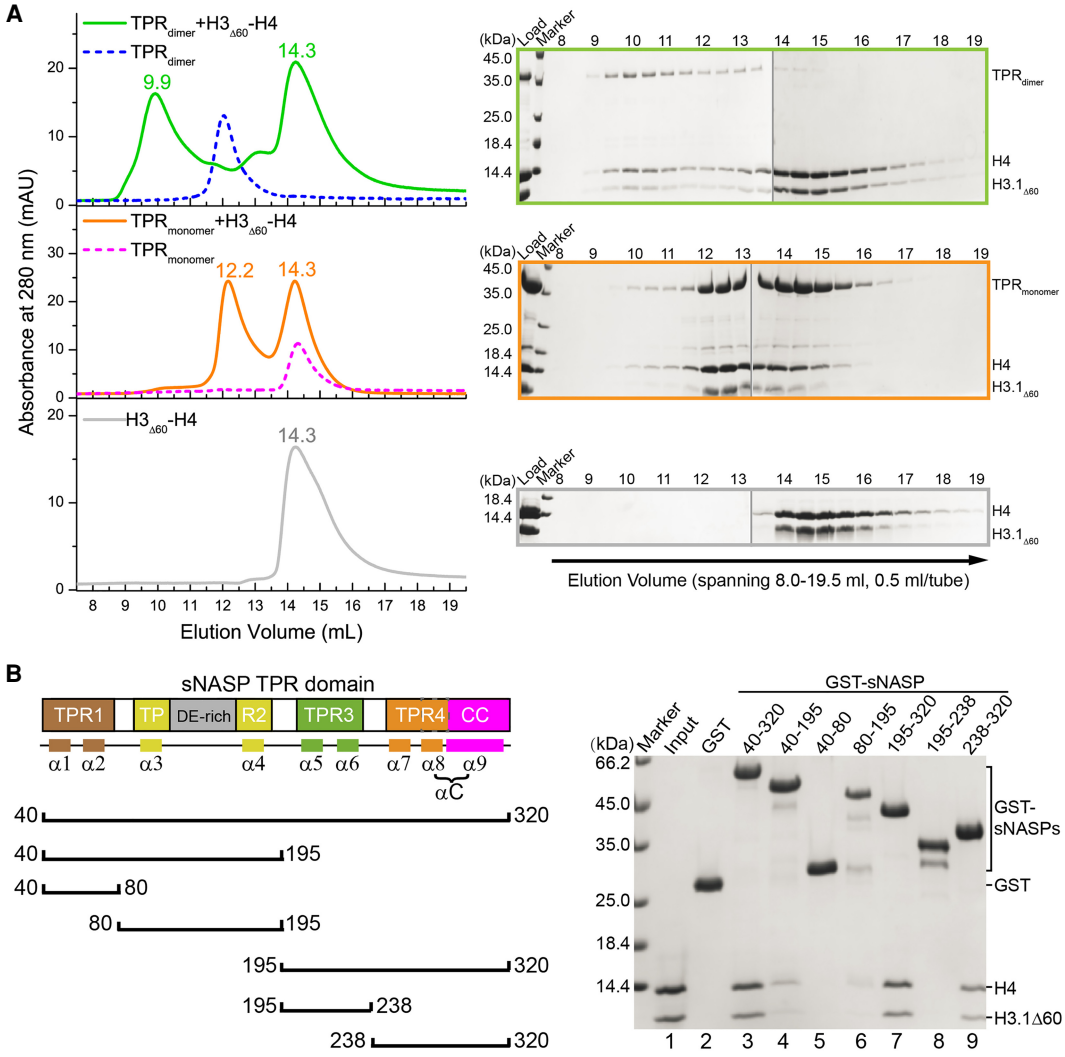

Figure 6. Histone binding mode of sNASP without ASF1. (*A*, *left* panels) Gel filtration detection of complex formation of H3.1Δ60–H4 (*bottom* panel) with dimeric or monomeric sNASP, shown in the *top* and *middle* panels, respectively. Elution profiles of sNASP dimer and monomer without histone bound, shown in blue and magenta dashed lines, respectively, are superimposed for reference. Peak positions (in milliliters) are labeled. (*Right* panels) SDS-PAGE analysis of 0.5-mL fractions spanning 8.0–19.5 mL corresponding to the three column runs shown in the *left* panels. Each gel panel was assembled from two gels with their boundary indicated by a thin vertical gray line. (*B*) Mapping of H3–H4 binding regions within sNASP. (*Left* panel) Schematic drawing of seven sNASP fragments used for GST pull-down with H3.1Δ60-H4. (*Right* panel) SDS-PAGE detection of sNASP elements interacting with the H3.1Δ60–H4 complex.

promiscuous interaction with cellular proteins, and erroneous and premature binding to nucleic acids. Histone chaperones are a mechanism to safeguard histones from these adverse effects and facilitate their correct functions. A diverse set of histone chaperones is involved in distinct functions of histones, including protein folding, histone storage, post-transcriptional modifications, nuclear import, and nucleosome assembly. Increasing evidences suggest that histone chaperones play more active roles than merely serving as histone escorts, and the manners by which histone chaperones bind histones often determine the outcome of histone functions. NASP is a major histone H3–H4 chaperone with diverse functions both in the cytoplasm and in the nucleus. However, how it binds histones H3 and H4 has been enigmatic, and lack of this knowledge prevented mechanistic understandings of its roles in the histone H3–H4 complex.

In this study, we first showed that the bacterially expressed sNASP TPR domain exists in both monomeric and dimeric forms, and full-length sNASP expressed in HEK293 cells also appears to have two forms, although the monomeric form appears to be more abundant. The structure shows that the dimeric sNASP TPR domain is formed through a drastic conformational switch of the very C-terminal helix, α9, which instead of folding back to pack with its own α8, straightened up to become part of a long, continuous helix that interacts with the corresponding region of another sNASP molecule. Nevertheless, both forms of sNASP bind histones H3–H4, whether in the presence or absence of ASF1. Apparently,

each TPR domain can independently bind histone H3–H4; our gel filtration analysis showed that the dimeric sNASP forms a defined complex with H3–H4 when ASF1 is present, consistent with a 2:2 stoichiometry (Fig. 3A). When ASF1 is absent, the dimeric sNASP forms a larger complex with H3Δ60–H4 (Fig. 6A); a 2:4 complex is possible, although we cannot rule out the possibility of a 2:2 complex, especially when H3 and H4 tails are intact, as the association of sNASP with H3–H4 in the absence of ASF1 is heterogeneous (Supplemental Fig. S6).

Both dimeric and monomeric forms of sNASP can facilitate nucleosome assembly in vitro. However, deletion of the long C-terminal helix, including the coiled-coil domain or removal of the coiled-coil domain only (Osakabe et al. 2010), both of which incapacitate dimer formation of sNASP, impairs the nucleosome assembly ability of sNASP. It is possible that dimerization of sNASP is needed for the nucleosome assembly; however, an alternative possibility is that amino acids located on the coiled-coil domain, whether in an extended conformation in a dimer or when it folds back in a monomer, play important roles in the process of depositing histones onto DNA during nucleosome assembly. Further in-depth studies are needed to unveil the functional consequences of sNASP dimerization.

Our study revealed that sNASP binds histone H3–H4 principally via the N-terminal tail of histone H3 in the presence of ASF1. A previous study found that an isolated histone H3 fragment encompassing the N-terminal tail and α1 of the histone fold domain can interact with sNASP (Cook et al. 2011). Our sNASP–ASF1A–H3–H4 structure shows that the H3 region spanning residues 40–57 interacts extensively with the convex surface region formed by TPR1–TPR3. The sNASP-interacting region in H3 includes the αN helix that is involved in interaction with DNA in the nucleosome. It is interesting that αN is partially unwound in the sNASP complex with ASF1A–H3–H4. The only other occasion αN is seen unwound is when yeast Asf1–H3–H4 is bound to Rtt109 for H3K56 acetylation (Zhang et al. 2018). These observations indicate that conformational flexibility of the H3 αN region is important for its functions in predepositional processes. Other than histone H3, a C-terminal region of H4 (including a short β strand that interacts with ASF1A via antiparallel β-pairing and the following C-terminal tail) also contacts the TPR3 and TPR4 region of sNASP. Curiously, deletion of this region of histone H4 does not disrupt the interaction between H3–H4 and sNASP, but ASF1A is evicted upon sNASP binding. Our interpretation is that, with the removal of the C-terminal region of H4, sNASP competes favorably with the remaining ASF1A binding site located on the loop connecting α2–α3 and an α3 portion of histone H3. This region of histone H3 is critical for homodimerization of H3; namely, tetramerization of H3–H4.

It is interesting that there is a separate sNASP binding site located on the C-terminal region of H3, in addition to the one located at the N-terminal region of H3. This finding is consistent with the results of two earlier studies, wherein an isolated α3 of histone H3 was shown to interact with sNASP (Bowman et al. 2016, 2017). The presence of two H3–H4 binding sites in sNASP is intriguing for understanding the mechanism of histone transfer between different chaperones. We may picture that the simultaneous presence of two different histone binding modes leads to multivalent, heterogeneous sNASP–H3–H4 complexes, enabling sNASP to maintain soluble histone pools in cytosol. On the arrival of ASF1, it blocks the second binding site of sNASP in H3–H4 and results in a homogenous sNASP–ASF1–H3–H4 complex, leaving only the N-terminal tail of H3 to interact with sNASP. This quaternary complex can then bind HAT1-RbAp46 to form the major soluble complex that is ready to be translocated into the nucleus, where ASF1 will eventually leave the major soluble complex with histones H3–H4 (Liu and Churchill 2012). The binding of HAT1-RbAp46 may sequester the N-terminal tail of histone H3 from sNASP, and triggers the transfer of H3–H4 to ASF1 upon completion of histone H4 acetylation by HAT1 (Li et al. 2014).

Materials and methods

Plasmid construction

The cDNA encoding full-length human sNASP was amplified by PCR and cloned into a modified pcDNA-3.1 vector (Invitrogen), and the resulting plasmid, termed pCDNA3-sNASP-strep, expresses sNASP carrying a C-terminal strep tag. The TPR domain of sNASP (amino acids 40–320) was subcloned into a pGEX-6P-1 vector (GE Healthcare) or a pRSFDuet-His_6-SUMOtag vector, a modified pRSFDuet-1 vector (Novagen) with an N-terminal His_6-SUMO tag. Bacterial expression plasmid for covalently linking the human sNASP TPR domain (amino acids 40–320) and the ASF1A histone binding domain (HBD; amino acids 1–156) through a glycine–serine linker $(GGGGS)_4$ was constructed by inserting the in-frame sequence coding for the sNASP TPR–$(G_4S)_4$–ASF1A HBD cassette into a pRSFDuet-His_6-SUMOtag vector.

cDNA fragments encoding the histone binding domain (HBD) of human ASF1A (amino acids 1–172 or 1–156) were amplified by PCR and cloned into the pRSFDuet-1 or the pRSFDuet-His_6-SUMOtag vector, respectively. Full-length human histones H3.1 and H4 were coexpressed using a bicistronic plasmid, pCDFDuet1–H3.1–H4. Deletion mutants or point mutants of sNASP, H3.1, or H4 were generated with the KOD-Plus mutagenesis kit (Toyobo SMK-101) following the manufacturer's protocols and confirmed by DNA sequencing (Supplemental Table S1).

Protein expression and purification

sNASP fragments were expressed in *E. coli* BL21 CodonPlus (DE3) RIL cells cultured in LB medium at 37°C, followed by induction of protein production with the addition of 0.5 mM isopropyl β-D-1-thiogalactopyranoside (IPTG) for 4 h. Selenomethionine (SeMet)-substituted sNASP TPR protein was prepared by inhibition of the *E. coli* methionine biosynthesis pathway. Briefly, the pRSFDuet-His_6-SUMOtag-sNASP TPR plasmid was transformed into *E. coli* BL21 CodonPlus (DE3) cells, and the bacteria were cultured in the LB medium at 37°C. The cells were collected and cultured in the M9 minimal medium at 37°C, followed by addition of 25 mg/L SeMet (Acros Organics); Lys, Thr, and Phe at 100 mg/L; and Leu, Ile, and Val at 50 mg/L to inhibit the endogenous synthesis of methionine when the OD_{600} value of the culture reached 0.6. After incubation for 1 h, the temperature was reduced to 16°C and

protein expression was induced by the addition of IPTG to a final concentration of 0.3 mM, followed by further shaking for 36 h.

All purification steps were carried out at 4°C. The following procedures were used for purification of sNASP TPR domain or its mutants. Cell pellets were resuspended in 5 vol of the binding buffer A with 20 mM Tris-HCl (pH 7.5), 500 mM NaCl, 20 mM imidazole, and 1 mM phenylmethylsulphonyl fluoride (PMSF), before lysing by sonication. Cell debris were removed by centrifugation, and the supernatant was incubated for 1 h at 4°C with Ni^{2+}-NTA agarose resins pre-equilibrated with buffer A, followed by washing the resins three times with buffer A. The bound proteins were eluted with buffer B (20 mM Tris-HCl at pH 7.5, 500 mM NaCl, 500 mM imidazole) and immediately supplemented with 1 mM each ethylenediaminetetraacetic acid (EDTA) and dithiothreitol (DTT). After removing the His_6-SUMO tag by using Ulp1 (SUMO protease), the protein was further purified on a HiLoad 16/60 Superdex 200 column (GE Healthcare) in buffer C (20 mM Tris-HCl at pH 7.5, 100 mM NaCl, 1 mM DTT). Elution fractions were analyzed by SDS-PAGE, and the fractions enriched with the desired proteins were pooled and concentrated to ~30 mg/mL by ultrafiltration and stored at −80°C before use.

Full-length sNASP was expressed in suspension culture of HEK293F cells in the SMM 293T-II medium (Sino Biological, Inc.). A total of 300 mL of HEK293F cells was transfected with 300 μg of pcDNA3-sNASP-strep plasmid plus 600 μg of linear polyethylenimine (PEI) (Polysciences), and cells were harvested at 48 h after transfection. The sNASP-strep protein was purified through successive steps of affinity purification with Strep-TactinXT beads (IBA Life Science), ion exchange with a heparin column (GE Healthcare), and size exclusion chromatography with a Superdex 200 Increase 10/300 GL column (GE Healthcare) in buffer D (20 mM Tris-HCl at pH 7.5, 500 mM NaCl, 5% glycerol, 1 mM DTT).

The complex of the sNASP TPR-ASF1A fusion protein with histones H3.1 and H4 was produced by coexpression of the pRSFDeut-His_6-SUMOtag-sNASP TPR-$(G_4S)_4$-ASF1A HBD plasmid and the pCDFDuet1–H3.1–H4 plasmid in *E. coli* BL21 CodonPlus (DE3) RIL cells. Production of the protein complex was induced with 0.5 mM IPTG for 4 h at 37°C. The protein complex was first purified on Ni^{2+}-NTA agarose resins. After removing the His_6-SUMO tag through digestion with Ulp1, the protein complex was first purified on a heparin column (GE Healthcare), followed by a HiLoad 16/60 Superdex 200 column (GE Healthcare) in buffer C (20 mM Tris-HCl at pH7.5, 100 mM NaCl, 1 mM DTT). Highly purified samples were pooled and concentrated to ~25 mg/mL and stored at −80°C.

ASF1A proteins were expressed in bacterial cells using the pRSFDuet-His_6-$ASF1A_{1–172}$ or the pRSFDuet-His_6-SUMOtag-$ASF1A_{1–156}$ plasmids for 4 h at 37°C with 0.5 mM IPTG. After purification with Ni^{2+}-NTA resins, the His_6-$ASF1A_{1–172}$ protein was directly eluted and further purified through a sizing column, whereas for His_6-SUMOtag-$ASF1A_{1–156}$, the His_6-SUMO tag was removed on the column, and the $ASF1A_{1–156}$ protein in the flow-through was collected and further purified in the sizing column. Histones H3.1–H4 were coexpressed using the pCDFDuet1–H3.1–H4 plasmid in *E. coli* cells for 4 h at 37°C with 0.5 mM IPTG. Histone complexes were first purified by ion exchange column using a 5-mL SP column (GE Healthcare), and further purified through a gel filtration column at 2 M NaCl. H3.1–H4 mutant complexes were expressed and purified following the same procedure.

Assembly of wild-type and mutant ASF1A–H3.1–H4 complexes was carried out by mixing H3.1–H4 and His_6-$ASF1A_{1–172}$ or $ASF1A_{1–156}$ at a 1:2 molar ratio for 30 min on ice, and loading onto a HiLoad 16/60 Superdex 200 (GE Healthcare) gel filtration column in buffer D (20 mM Tris-HCl at pH 7.5, 500 mM NaCl, 5% glycerol, 1 mM DTT). Fractions enriched with the ternary complex were pooled and concentrated to ~10 mg/mL.

Crystallization, data collection, and structure determination

Native crystals of the dimeric sNASP TPR domain were obtained by mixing 1.0 μL of protein (15–18 mg/mL) with 1.0 μL of reservoir solution containing 0.1 M sodium cacodylate (pH 6.5), 32% (v/v) PEG 300, and 0.2 M calcium acetate. The SeMet-substituted sNASP TPR domain was crystallized in 0.1 M MES (pH 6.5), 30% (v/v) PEG300, and 0.18 M calcium acetate at a concentration of 12–15 mg/mL. The $sNASP_{40–320}$–$(G_4S)_4$–$ASF1A_{1–156}$–H3.1–H4 complex protein at a concentration of 10–12 mg/mL was crystallized in 18% (v/v) tacsimate (pH 5.0), and 11% (w/v) PEG2000MME. All crystals were grown by sitting-drop vapor diffusion at 4°C. Cryogenic data collection was performed with cryoprotectants prepared by supplementing the crystallization mother liquors with 15% glycerol before flash-freezing in liquid nitrogen.

For structural determination of the dimeric sNASP TPR domain, X-ray diffraction data were collected at the Shanghai Synchrotron Radiation Facility (SSRF) beamline BL17U equipped with a Quantum 315r CCD detector (ADSC) using a wavelength of 0.97915 Å. Data were processed using the HKL2000 software package (Otwinowski and Minor 1997). Four Se sites were identified with SHELXD (Collaborative Computational Project, Number 4 1994) using the 3.6 Å SeMet data set. Refinement of the heavy atom substructure, phasing, and density modification was performed using PHENIX (Adams et al. 2010). The experimentally determined phase was then extended to the 2.9 Å resolution native data set. The initial model was manually built with COOT (Emsley and Cowtan 2004), and the model was improved by iterative cycles of refinement and model adjustment. The final structure had R_{work} and R_{free} values of 0.187 and 0.223, respectively, and good stereochemical quality, with 97.2% and 2.8% of the residues in the favored and allowed regions of the Ramachandran plot, respectively. The ordered structure contained residues 40–103 and 167–320 of sNASP TPR. Residues 104–166 of TPR2 were rich in acidic residues and had no clear electron density, and thus were not included the final model.

Crystal diffraction data for the sNASP–ASF1–H3–H4 complex were also collected at SSRF beamline BL17U at a wavelength of 0.97913 Å using a Dectris Eiger 16 M detector, and processed with the HKL2000 package. The complex structure was determined by molecular replacement using PHASER with the structures of ASF1A–H3–H4 (PDB: 2IO5) and the structure of the sNASP TPR domain encompassing the α1–α7 region as the search models. The structure was then manually adjusted using COOT and refined in PHENIX. The final structure contained residues 40–103 and 167–320 of the sNASP TPR domain, residues 40–135 of histone H3.1, residues 23–102 of histone H4, and residues 1–154 of ASF1A. The refined model had satisfactory *R*-values (R_{work}/R_{free} = 0.165/0.203) and good Ramachandran statistics (97.4% favored and 2.6% allowed). Finally, the models were validated with MolProbity (Chen et al. 2010). Detailed statistics for data collection and structure refinement are shown in Table 1. Structural figures were prepared using PyMOL (Schrödinger LLC).

Atomic coordinates and structure factors have been deposited in PDB with accession numbers 7V6P and 7V6Q for the sNASP TPR domain and the sNASP–ASF1A–H3–H4 complex, respectively.

Molecular size analysis by gel filtration

The sNASP TPR domain was loaded onto a Superdex 200 Increase 10/300 GL column (GE Healthcare) equilibrated in a buffer

containing 20 mM Tris-HCl (pH 7.5), 500 mM NaCl, and 5% glycerol. Peak 1 contained fraction eluted between 11.5 and 13.0 mL, and peak 2 contained fractions eluted between 14.0 and 15.5 mL. Samples of both peak 1 and peak 2 were reloaded onto the sizing column for further analysis. Analyses of various protein complexes and individual components were carried out using the samples prepared as described before, and in the cases of testing binding with sNASP TPR domain, other components were added in roughly twofold excess. The loading samples were generally diluted to ~1–3 mg/mL, and a total volume of 0.5 mL in 20 mM Tris-HCl (pH 7.5), 500 mM NaCl, and 5% glycerol. The samples were then injected at 0.4 mL/min onto a Superdex 200 Increase 10/300 GL column (GE Healthcare). Elution fractions between 8.0 and 19.5 mL were pooled and analyzed by SDS-PAGE and stained with Coomassie blue. The gel filtration chromatograms were plotted by OriginPro 8.0 (OriginLab Corporation).

Analytical ultracentrifugation (AUC)

Sedimentation velocity experiments were carried out in a Beckman Coulter ProteomeLab XL-I analytical ultracentrifuge with absorbance detection. Samples were prepared in a buffer containing 20 mM Tris-HCl (pH 7.5), 500 mM NaCl, and 1 mM EDTA. Samples of the sNASP TPR domain from peak 1 and peak 2, and peak 2 of full-length sNASP, all at ~1 mg/mL in a total volume of 400 µL, were loaded into the cell chamber against buffer blank and spun at 55,000 rpm for 7 h at 20°C. Data were analyzed using the c(M) model of molecular mass distribution in Sedfit (Schuck 2000).

Topological assay for nucleosome assembly

DNA supercoiling assays were performed as described previously (Osakabe et al. 2010) with the following modifications. Relaxed DNA template was prepared by combining ϕX174 RF I DNA (NEB N3021S) with excess DNA topoisomerase I (TaKaRa 2240A) in the assembly buffer (10 mM Tris-HCl at pH 7.5, 125 mM NaCl, 2 mM $MgCl_2$, 0.5 mM DTT, 0.1 mg/mL BSA) for 1 h at 37°C and kept at room temperature ready for use. Histone octamers (200 ng) were preincubated with 250/500 ng of yNAP1, full-length sNASP, sNASP TPR monomer, sNASP TPR dimer, or sNASP TPRΔαC (2.5-fold/fivefold to octamer), respectively, in the assembly buffer for 30 min at 37°C. To initiate the assembly reaction, 100 ng of relaxed plasmid DNA was added to the chaperone–histone mixture and incubated for 90 min at 37°C. The standard 25-µL chromatin assembly reaction was stopped by adding EDTA to 20 mM and SDS to 0.5%, with an additional 0.5 mg/mL proteinase K, and incubation for 15 min at 55°C followed by phenol-chloroform extraction. The DNA samples were analyzed on a 1% agarose gel in 1× TAE buffer (40 mM Tris-acetate, 1 mM EDTA) for 4 h at 90 V with ethidium bromide (EB) staining.

GST pull-downs

For pull-down experiments between the GST-sNASP TPR domain and ASF1A–H3.1–H4 proteins, 3 µg of GST, GST-sNASP TPR, or its mutants were immobilized on 5 µL of glutathione Sepharose 4B resin, which was then mixed with 5 µg of ASF1A–H3.1–H4 or its mutants in 500 µL of the binding buffer (20 mM Tris-HCl at pH 7.5, 300 mM NaCl, 5 mM 2-mercaptoethanol, 0.02% NP-40, 1 mM EDTA), and the mixture was rotated overnight at 4°C. The resins were then washed five times with 1 mL of binding buffer with 500 mM NaCl. Bound proteins were eluted in SDS sample buffer, separated on a 15% SDS-PAGE gel, and stained with Coomassie blue. GST pull-down experiments between GST-sNASP fragments and WT or mutant H3.1–H4 complexes were performed following the same procedure.

Cellular targeting assay

The A03_1 cell line was generated by insertion of 256 repeats of LacO operators into the genome of CHO cells (Robinett et al. 1996). The cells were cultured in F-12 Ham's medium (Gibco) supplemented with 10% FBS (AusGeneX) and 1% penicillin/streptomycin (Thermo Fisher). For cellular localization detection, cDNAs expressing full-length sNASP and its mutants were subcloned into a pmCherry-LacI vector, while the cDNAs of H3.1 or H4, as well as their mutants, were inserted into the pEGFP-N1 vector.

For LacI–LacO targeting experiments, A03_1 cell transfection and confocal fluorescence imaging procedures were performed as previously described (Liu et al. 2012). In brief, cells seeded on glass coverslips in a 24-well plate were cotransfected with plasmids pmCherry-LacI-sNASP and pEGFP-N1-H3.1 or pEGFP-N1-H4 (WT or mutants) using the Lipofectamine 3000 transfection kit (Thermo Fisher) according to the manufacturer's instructions. At 48 h after transfection, cells were washed with PBS and fixed with 4% formaldehyde (Sigma) for 15 min on ice. Then cells were washed again and stained with DAPI (Sigma) for 15 min at room temperature. A Nikon AI confocal microscope was used to analyze the fluorescence signals under a 60× oil immersion lens. Statistical error bars for colocalizing mCherry and EGFP foci in A03_1 cells were derived from three sets of 50 randomly selected cells, and represent the standard error of the mean (± SEM).

Competing interest statement

The authors declare no competing interests.

Acknowledgments

We thank staff scientists at the Shanghai Synchrotron Radiation Facility beamlines BL17U and BL19U for assistance for X-ray data collection, and Dr. Xiaoxia Yu for technical support in handling AUC. This work was supported in part by grants from the Natural Science Foundation of China (91853204, 31991162, and 31521002), the Ministry of Science and Technology of China (2017YFA0504202, 2018YFE0203300, 2017YFA0506600, and 2019YFA0508900), and the Strategic Priority Research Program of Chinese Academy of Sciences (XDB37010101). C.-P.L. is supported by the Youth Innovation Promotion Association of the Chinese Academy of Sciences (2018125).

Author contributions: R.-M.X. conceived the project. C.-P.L. performed protein expression, purification, crystallization, and structure determination. C.-P.L and M.W. collected X-ray data and refined models. C.-P.L. performed AUC experiments, GST pull-downs, and gel filtration experiments. W.J. performed fluorescence colocalization experiments and protein expression in 293F cells. J.C. assisted and provided support of all experiments. J.H. performed the supercoiling assays under the supervision of G.L. C.-P.L. and R.-M.X. wrote the manuscript, and all authors discussed the results and contributed to the final manuscript.

References

Adams PD, Afonine PV, Bunkóczi G, Chen VB, Davis IW, Echols N, Headd JJ, Hung LW, Kapral GJ, Grosse-Kunstleve RW, et al. 2010. PHENIX: a comprehensive Python-based system for macromolecular structure solution. *Acta Crystallogr D Biol Crystallogr* **66:** 213–221. doi:10.1107/S0907444909052925

Ai X, Parthun MR. 2004. The nuclear Hat1p/Hat2p complex: a molecular link between type B histone acetyltransferases and chromatin assembly. *Mol Cell* **14:** 195–205. doi:10.1016/S1097-2765(04)00184-4

Alekseev OM, Richardson RT, Alekseev O, O'Rand MG. 2009. Analysis of gene expression profiles in HeLa cells in response to overexpression or siRNA-mediated depletion of NASP. *Reprod Biol Endocrinol* **7:** 45. doi:10.1186/1477-7827-7-45

Alekseev OM, Richardson RT, Tsuruta JK, O'Rand MG. 2011. Depletion of the histone chaperone tNASP inhibits proliferation and induces apoptosis in prostate cancer PC-3 cells. *Reprod Biol Endocrinol* **9:** 50. doi:10.1186/1477-7827-9-50

Alvarez F, Muñoz F, Schilcher P, Imhof A, Almouzni G, Loyola A. 2011. Sequential establishment of marks on soluble histones H3 and H4. *J Biol Chem* **286:** 17714–17721. doi:10.1074/jbc.M111.223453

Apta-Smith MJ, Hernandez-Fernaud JR, Bowman AJ. 2018. Evidence for the nuclear import of histones H3.1 and H4 as monomers. *EMBO J* **37:** e98714. doi:10.15252/embj.201798714

Bamford S, Dawson E, Forbes S, Clements J, Pettett R, Dogan A, Flanagan A, Teague J, Futreal PA, Stratton MR, et al. 2004. The COSMIC (catalogue of somatic mutations in cancer) database and website. *Br J Cancer* **91:** 355–358. doi:10.1038/sj.bjc.6601894

Bowman A, Lercher L, Singh HR, Zinne D, Timinszky G, Carlomagno T, Ladurner AG. 2016. The histone chaperone sNASP binds a conserved peptide motif within the globular core of histone H3 through its TPR repeats. *Nucleic Acids Res* **44:** 3105–3117. doi:10.1093/nar/gkv1372

Bowman A, Koide A, Goodman JS, Colling ME, Zinne D, Koide S, Ladurner AG. 2017. sNASP and ASF1A function through both competitive and compatible modes of histone binding. *Nucleic Acids Res* **45:** 643–656. doi:10.1093/nar/gkw892

Campos EI, Fillingham J, Li G, Zheng H, Voigt P, Kuo WH, Seepany H, Gao Z, Day LA, Greenblatt JF, et al. 2010. The program for processing newly synthesized histones H3.1 and H4. *Nat Struct Mol Biol* **17:** 1343–1351. doi:10.1038/nsmb.1911

Chen VB, Arendall WB III, Headd JJ, Keedy DA, Immormino RM, Kapral GJ, Murray LW, Richardson JS, Richardson DC. 2010. *Molprobity*: all-atom structure validation for macromolecular crystallography. *Acta Crystallogr D Biol Crystallogr* **66:** 12–21. doi:10.1107/S0907444909042073

Collaborative Computational Project, Number 4. 1994. The CCP4 suite: programs for protein crystallography. *Acta Crystallogr D Biol Crystallogr* **50:** 760–763. doi:10.1107/S0907444994003112

Cook AJ, Gurard-Levin ZA, Vassias I, Almouzni G. 2011. A specific function for the histone chaperone NASP to fine-tune a reservoir of soluble H3–H4 in the histone supply chain. *Mol Cell* **44:** 918–927. doi:10.1016/j.molcel.2011.11.021

Das C, Tyler JK, Churchill ME. 2010. The histone shuffle: histone chaperones in an energetic dance. *Trends Biochem Sci* **35:** 476–489. doi:10.1016/j.tibs.2010.04.001

Dunleavy EM, Pidoux AL, Monet M, Bonilla C, Richardson W, Hamilton GL, Ekwall K, McLaughlin PJ, Allshire RC. 2007. A NASP (N1/N2)-related protein, Sim3, binds CENP-A and is required for its deposition at fission yeast centromeres. *Mol Cell* **28:** 1029–1044. doi:10.1016/j.molcel.2007.10.010

Emsley P, Cowtan K. 2004. *Coot*: model-building tools for molecular graphics. *Acta Crystallogr D Biol Crystallogr* **60:** 2126–2132. doi:10.1107/S0907444904019158

English CM, Adkins MW, Carson JJ, Churchill ME, Tyler JK. 2006. Structural basis for the histone chaperone activity of Asf1. *Cell* **127:** 495–508. doi:10.1016/j.cell.2006.08.047

Finn RM, Browne K, Hodgson KC, Ausió J. 2008. sNASP, a histone H1-specific eukaryotic chaperone dimer that facilitates chromatin assembly. *Biophys J* **95:** 1314–1325. doi:10.1529/biophysj.108.130021

Finn RM, Ellard K, Eirín-López JM, Ausió J. 2012. Vertebrate nucleoplasmin and NASP: egg histone storage proteins with multiple chaperone activities. *FASEB J* **26:** 4788–4804. doi:10.1096/fj.12-216663

Grover P, Asa JS, Campos EI. 2018. H3–H4 histone chaperone pathways. *Annu Rev Genet* **52:** 109–130. doi:10.1146/annurev-genet-120417-031547

Gurard-Levin ZA, Quivy JP, Almouzni G. 2014. Histone chaperones: assisting histone traffic and nucleosome dynamics. *Annu Rev Biochem* **83:** 487–517. doi:10.1146/annurev-biochem-060713-035536

Han J, Zhou H, Horazdovsky B, Zhang K, Xu RM, Zhang Z. 2007. Rtt109 acetylates histone H3 lysine 56 and functions in DNA replication. *Science* **315:** 653–655. doi:10.1126/science.1133234

Jasencakova Z, Scharf AN, Ask K, Corpet A, Imhof A, Almouzni G, Groth A. 2010. Replication stress interferes with histone recycling and predeposition marking of new histones. *Mol Cell* **37:** 736–743. doi:10.1016/j.molcel.2010.01.033

Kleinschmidt JA, Franke WW. 1982. Soluble acidic complexes containing histones H3 and H4 in nuclei of Xenopus laevis oocytes. *Cell* **29:** 799–809. doi:10.1016/0092-8674(82)90442-1

Kleinschmidt JA, Fortkamp E, Krohne G, Zentgraf H, Franke WW. 1985. Co-existence of two different types of soluble histone complexes in nuclei of *Xenopus laevis* oocytes. *J Biol Chem* **260:** 1166–1176. doi:10.1016/S0021-9258(20)71223-8

Li Y, Zhang L, Liu T, Chai C, Fang Q, Wu H, Agudelo Garcia PA, Han Z, Zong S, Yu Y, et al. 2014. Hat2p recognizes the histone H3 tail to specify the acetylation of the newly synthesized H3/H4 heterodimer by the Hat1p/Hat2p complex. *Genes Dev* **28:** 1217–1227. doi:10.1101/gad.240531.114

Liu WH, Churchill ME. 2012. Histone transfer among chaperones. *Biochem Soc Trans* **40:** 357–363. doi:10.1042/BST20110737

Liu CP, Xiong C, Wang M, Yu Z, Yang N, Chen P, Zhang Z, Li G, Xu RM. 2012. Structure of the variant histone H3.3-H4 heterodimer in complex with its chaperone DAXX. *Nat Struct Mol Biol* **19:** 1287–1292. doi:10.1038/nsmb.2439

Liu H, Zhang M, He W, Zhu Z, Teng M, Gao Y, Niu L. 2014. Structural insights into yeast histone chaperone Hif1: a scaffold protein recruiting protein complexes to core histones. *Biochem J* **462:** 465–473. doi:10.1042/BJ20131640

Loyola A, Bonaldi T, Roche D, Imhof A, Almouzni G. 2006. PTMs on H3 variants before chromatin assembly potentiate their final epigenetic state. *Mol Cell* **24:** 309–316. doi:10.1016/j.molcel.2006.08.019

Luger K, Mäder AW, Richmond RK, Sargent DF, Richmond TJ. 1997. Crystal structure of the nucleosome core particle at 2.8 Å resolution. *Nature* **389:** 251–260. doi:10.1038/38444

Masumoto H, Hawke D, Kobayashi R, Verreault A. 2005. A role for cell-cycle-regulated histone H3 lysine 56 acetylation in the DNA damage response. *Nature* **436:** 294–298. doi:10.1038/nature03714

Nabeel-Shah S, Ashraf K, Pearlman RE, Fillingham J. 2014. Molecular evolution of NASP and conserved histone H3/H4

transport pathway. *BMC Evol Biol* **14:** 139. doi:10.1186/1471-2148-14-139

Natsume R, Eitoku M, Akai Y, Sano N, Horikoshi M, Senda T. 2007. Structure and function of the histone chaperone CIA/ASF1 complexed with histones H3 and H4. *Nature* **446:** 338–341. doi:10.1038/nature05613

O'Rand MG, Richardson RT, Zimmerman LJ, Widgren EE. 1992. Sequence and localization of human NASP: conservation of a Xenopus histone-binding protein. *Dev Biol* **154:** 37–44. doi:10.1016/0012-1606(92)90045-I

Osakabe A, Tachiwana H, Matsunaga T, Shiga T, Nozawa RS, Obuse C, Kurumizaka H. 2010. Nucleosome formation activity of human somatic nuclear autoantigenic sperm protein (sNASP). *J Biol Chem* **285:** 11913–11921. doi:10.1074/jbc.M109.083238

Otwinowski Z, Minor W. 1997. Processing of X-ray diffraction data collected in oscillation mode. *Methods Enzymol* **276:** 307–326. doi:10.1016/S0076-6879(97)76066-X

Pardal AJ, Fernandes-Duarte F, Bowman AJ. 2019. The histone chaperoning pathway: from ribosome to nucleosome. *Essays Biochem* **63:** 29–43. doi:10.1042/EBC20180055

Richardson RT, Batova IN, Widgren EE, Zheng LX, Whitfield M, Marzluff WF, O'Rand MG. 2000. Characterization of the histone H1-binding protein, NASP, as a cell cycle-regulated somatic protein. *J Biol Chem* **275:** 30378–30386. doi:10.1074/jbc.M003781200

Richardson RT, Alekseev OM, Grossman G, Widgren EE, Thresher R, Wagner EJ, Sullivan KD, Marzluff WF, O'Rand MG. 2006. Nuclear autoantigenic sperm protein (NASP), a linker histone chaperone that is required for cell proliferation. *J Biol Chem* **281:** 21526–21534. doi:10.1074/jbc.M603816200

Robinett CC, Straight A, Li G, Willhelm C, Sudlow G, Murray A, Belmont AS. 1996. In vivo localization of DNA sequences and visualization of large-scale chromatin organization using lac operator/repressor recognition. *J Cell Biol* **135:** 1685–1700. doi:10.1083/jcb.135.6.1685

Rose A, Meier I. 2004. Scaffolds, levers, rods and springs: diverse cellular functions of long coiled-coil proteins. *Cell Mol Life Sci* **61:** 1996–2009. doi:10.1007/s00018-004-4039-6

Ruiz-Carrillo A, Wangh LJ, Allfrey VG. 1975. Processing of newly synthesized histone molecules. *Science* **190:** 117–128. doi:10.1126/science.1166303

Schuck P. 2000. Size-distribution analysis of macromolecules by sedimentation velocity ultracentrifugation and lamm equation modeling. *Biophys J* **78:** 1606–1619. doi:10.1016/S0006-3495(00)76713-0

Sobel RE, Cook RG, Perry CA, Annunziato AT, Allis CD. 1995. Conservation of deposition-related acetylation sites in newly synthesized histones H3 and H4. *Proc Natl Acad Sci* **92:** 1237–1241. doi:10.1073/pnas.92.4.1237

Tyler JK, Adams CR, Chen SR, Kobayashi R, Kamakaka RT, Kadonaga JT. 1999. The RCAF complex mediates chromatin assembly during DNA replication and repair. *Nature* **402:** 555–560. doi:10.1038/990147

Verreault A, Kaufman PD, Kobayashi R, Stillman B. 1998. Nucleosomal DNA regulates the core-histone-binding subunit of the human Hat1 acetyltransferase. *Curr Biol* **8:** 96–108. doi:10.1016/S0960-9822(98)70040-5

Wang H, Walsh ST, Parthun MR. 2008. Expanded binding specificity of the human histone chaperone NASP. *Nucleic Acids Res* **36:** 5763–5772. doi:10.1093/nar/gkn574

Wang H, Ge Z, Walsh ST, Parthun MR. 2012. The human histone chaperone sNASP interacts with linker and core histones through distinct mechanisms. *Nucleic Acids Res* **40:** 660–669. doi:10.1093/nar/gkr781

Xu F, Zhang K, Grunstein M. 2005. Acetylation in histone H3 globular domain regulates gene expression in yeast. *Cell* **121:** 375–385. doi:10.1016/j.cell.2005.03.011

Zhang M, Liu H, Gao Y, Zhu Z, Chen Z, Zheng P, Xue L, Li J, Teng M, Niu L. 2016. Structural insights into the association of Hif1 with histones H2A–H2B dimer and H3–H4 tetramer. *Structure* **24:** 1810–1820. doi:10.1016/j.str.2016.08.001

Zhang L, Serra-Cardona A, Zhou H, Wang M, Yang N, Zhang Z, Xu RM. 2018. Multisite substrate recognition in Asf1-dependent acetylation of histone H3 K56 by Rtt109. *Cell* **174:** 818–830.e11. doi:10.1016/j.cell.2018.07.005